Journal of Modern Optics

ISSN: 0950-0340 (Print) 1362-3044 (Online) Journal homepage: http://www.tandfonline.com/loi/tmop20

Experimental confirmation of the transversal symmetry breaking in laser profiles

Silvânia A. Carvalho, Stefano De Leo, José A. Oliveira-Huguenin & Ladário da Silva

To cite this article: Silvânia A. Carvalho, Stefano De Leo, José A. Oliveira-Huguenin & Ladário da Silva (2017) Experimental confirmation of the transversal symmetry breaking in laser profiles, Journal of Modern Optics, 64:3, 280-287, DOI: 10.1080/09500340.2016.1229511

To link to this article: http://dx.doi.org/10.1080/09500340.2016.1229511

JOURNAL OF MODERN OPTICS, 2017
VOL. 64, NO. 3, 280–287
http://dx.doi.org/10.1080/09500340.2016.1229511

Taylor & Francis
Taylor & Francis Group

Experimental confirmation of the transversal symmetry breaking in laser profiles

Silvânia A. Carvalho[a], Stefano De Leo[b], José A. Oliveira-Huguenin[c] and Ladário da Silva[c]

[a]Department of Mathematics, Physics and Computation, State University of Rio de Janeiro, Resende, Brazil; [b]Department of Applied Mathematics, State University of Campinas, Campinas, Brazil; [c]Department of Physics, Fluminense Federal University, Volta Redonda, Brazil

ABSTRACT

The Snell phase effects on the propagation of optical beams through dielectric blocks have been matter of recent theoretical studies. The effects of this phase on the laser profiles have been tested in our experiment. The data show an excellent agreement with the theoretical predictions confirming the axial spreading modification and the transversal symmetry breaking. The possibility to set, by rotating the dielectric blocks, different configurations allows to recover the transversal symmetry. Based on this experimental evidence, dielectric blocks can be used as alternative optical tools to control the beam profile.

ARTICLE HISTORY
Received 23 May 2016
Accepted 19 August 2016

KEYWORDS
Laser; transversal symmetry breaking; Snell phase

1. Introduction

Studies of the optical beam phase confirmed (*1*) or suggested deviations (*2*–*8*) from the law of geometrical optics (*9*, *10*). For example, the first-order Taylor expansion of the Snell phase represents an alternative method to calculate, by the stationary phase method (*1*), the optical path of light beams. In a recent work (*11*), the effects of the second-order Taylor expansion of the Snell phase on the beam profile was investigated and an analytical formula found for the transversal symmetry breaking and the axial spreading modification. If such theoretical predictions were confirmed by an experimental analysis, the use of the Snell phase in describing the optical beam propagation through dielectric blocks is not a matter of elegance in determining the optical path, but a necessity in correctly predicting the beam profile behavior. In this case, the importance of the Snell phase could not only be seen in confirming the law of geometrical optics (first-order term expansion) but also in predicting deviations from the original shape of our beam (second-order term expansion).

The beam profile control finds important applications in many research fields. In the mode matching of optical cavities, the adjustment of the beam width is crucial for a good luminous energy storage (*10*). An optical parametric oscillator needs a good mode matching in order to amplify the conversion of signal and idler beams, and to minimize the loose of squeezing by noise introduction (*12*, *13*). For the second harmonic generation in photonics crystal wave-guides, the mode matching should be carefully observed (*14*). Additionally, the trapping of charged and neutral atoms has played a fundamental role in atomic and molecular physics (*15*). The common trap used for storage devices at ultra-low energies is the dipole trap which relies on the electric dipole interaction with far-detuned lasers. The result is a structure to trap atoms in the region of high intensity of a focused beam (*16*, *17*). In this context, a controlled rotation of dielectric blocks sheds new light on fine tuning the axial spreading factor and, consequently, tuning of these optical systems in general. Thus, a device capable of controlling the beam width in a simple and precise way is of great importance for laser applications.

The aim of this paper is to experimentally detect the axial spreading modification and the breaking of transversal symmetry of gaussian beams propagating through dielectrics blocks. Our paper is organized as follows. Section 2 gives a brief exposition of the theoretical predictions and contains the analytical formula used to describe the outgoing beam. It is not our intention to present all the aspects of the theory leading to the analytical formula. For details, we refer the reader to (*11*). Section 3 discusses the experimental data, which show an excellent agreement with the theoretical predictions both for the transversal symmetry breaking and for the axial spreading modification. This suggests the possibility to control the laser beam profile by an appropriate dielectric blocks setup. The final section contains our conclusions and suggestions for future investigations.

CONTACT Stefano De Leo deleo@ime.unicamp.br

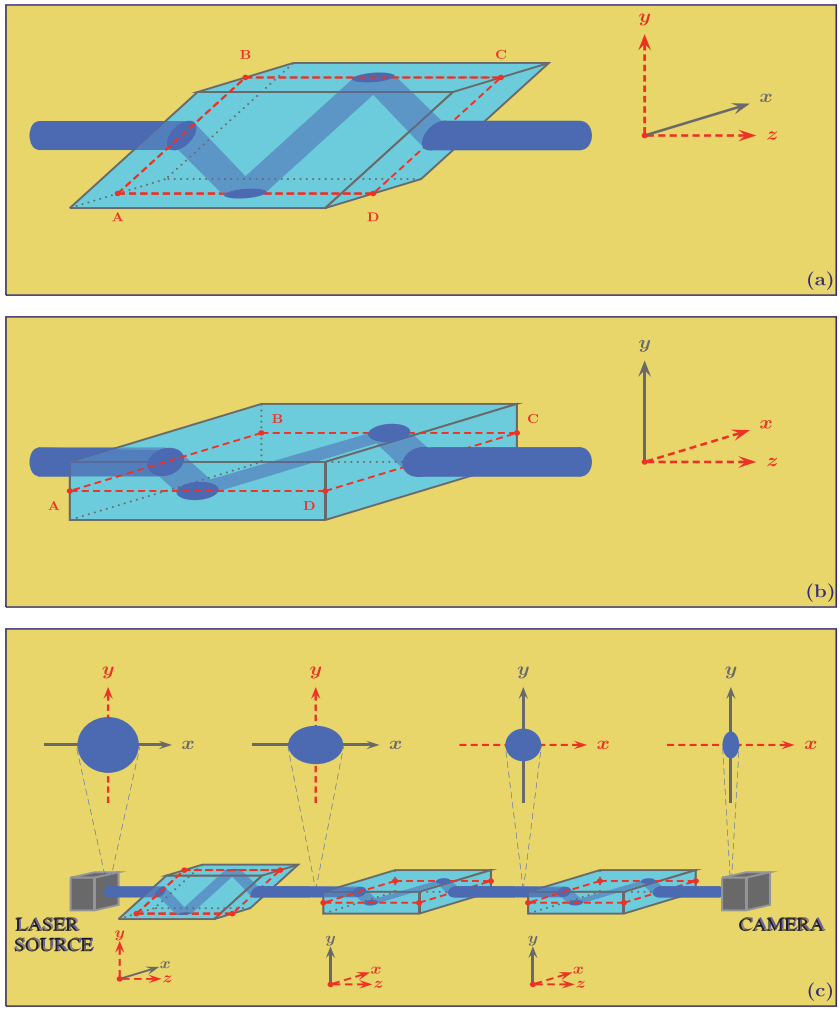

Figure 1. Experimental setup. The incoming beam propagate along the z-axial forming an angle of $\pi/4$ with the left interface of the dielectric blocks. In (a), the plane of propagation is the plane y-z and represents the configuration $M, N) = (0, 1)$. In (b), the block is clockwise rotated by an angle $\pi/2$ along the axial axis, configuration $(M, N) = (1, 0)$. In (c), we have the configuration $(M, N) = (2, 1)$. The transversal symmetry is recovered when the beam passes through the same number of blocks M and N.

2. Axial spreading and transversal symmetry breaking

Let us consider, an incoming gaussian beam whose intensity is given by

$$I_{\rm inc}(\boldsymbol{r}) = I_0 \left| \frac{\mathrm{w}_0^2}{4\pi} \int_{-\infty}^{+\infty} \mathrm{d}k_x \int_{-\infty}^{+\infty} \mathrm{d}k_y \, g(k_x, k_y) \times \exp\left[i \left(k_x x + k_y y + k_z z \right) \right] \right|^2, \qquad (1)$$

where $g(k_x, k_y) = \exp\left[-\left(k_x^2 + k_y^2 \right) \mathrm{w}_0^2 / 4 \right]$ and $k_z = \sqrt{k^2 - k_x^2 - k_y^2}$ $(k = 2\pi/\lambda)$.

For $\mathrm{w}_0 \gtrsim \lambda$, the beam divergence is relatively small and we can use the paraxial approximation, $k_z \approx k - (k_x^2 + k_y^2)/2k$, which allows to analytically integrate the expression for the intensity of the incident beam, Equation (1), obtaining the well-known expression describing the propagation of free gaussian beams

$$I_{\rm inc}(\boldsymbol{r}) = \frac{I_0 \, \mathrm{w}_0^2}{\mathrm{w}^2(z)} \exp\left[-2 \, \frac{x^2 + y^2}{\mathrm{w}^2(z)} \right], \qquad \mathrm{w}(z) = \mathrm{w}_0 \sqrt{1 + \left(\frac{\lambda \, z}{\pi \, \mathrm{w}_0^2} \right)^2}. \qquad (2)$$

After passing through N dielectric blocks like those drawn in Figure 1(a) and M dielectric blocks, clockwise rotated with respect to the previous ones by an angle $\pi/2$ along the z axis, (see Figure 1(b)),

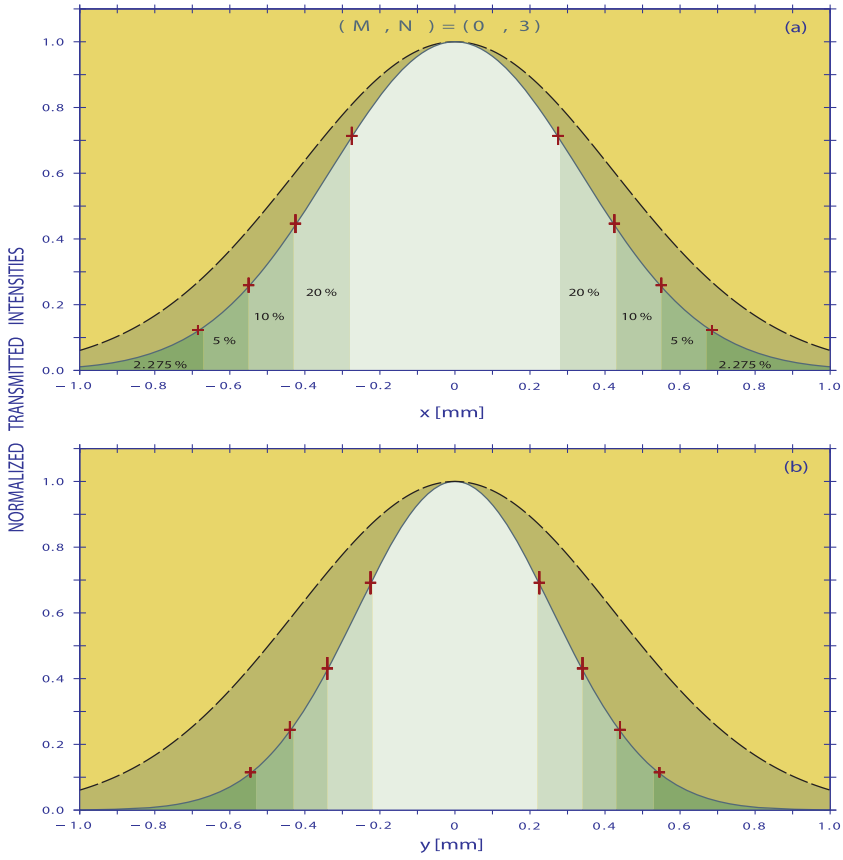

Figure 2. Transversal profiles of the normalized transmitted intensity. The dashed black lines represent the profiles for free propagation. The blue solid lines are the profiles for beams passing through the dielectric configuration $(M, N) = (0, 3)$. The breaking of symmetry between the x and y axis is clear and the axial spreading delay with respect to the free propagation is more evident for the transversal component y. The experimental data show an excellent agreement with the theoretical curves.

Table 1. We find the experimental beam widths obtained by the knife-method measurements done for power cuts of 2.275–97.725% (a), 5.0–95.0% (b), 10.0–90.0% (c), and 20.0–80.0% (d). The data show agreement with the theoretical widths.

KM	(M,N)	$x_{\mathrm{KM}}[\mu\mathrm{m}]$	$w_{\mathrm{Exp}}^{\mathrm{Snell},\perp}[\mu\mathrm{m}]$	$w_{\mathrm{Teo}}^{\mathrm{Snell},\perp}[\mu\mathrm{m}]$	$y_{\mathrm{KM}}[\mu\mathrm{m}]$	$w_{\mathrm{Exp}}^{\mathrm{Snell}}[\mu\mathrm{m}]$	$w_{\mathrm{Teo}}^{\mathrm{Snell}}[\mu\mathrm{m}]$
(a)	(0, 3)	685	685.0 ± 15.0	669.5 ± 12.4	545	545.0 ± 15.0	524.2 ± 9.5
	(1, 1)	695	695.0 ± 15.0	681.2 ± 12.6	690	690.0 ± 15.0	681.2 ± 12.6
(b)	(0, 3)	550	670.7 ± 18.3	669.5 ± 12.4	440	536.6 ± 18.3	524.2 ± 9.5
	(1, 1)	555	676.8 ± 18.3	681.2 ± 12.6	550	670.7 ± 18.3	681.2 ± 12.6
(c)	(0, 3)	425	664.1 ± 23.4	669.5 ± 12.4	340	531.3 ± 23.4	524.2 ± 9.5
	(1, 1)	430	671.9 ± 23.4	681.2 ± 12.6	430	671.9 ± 23.4	681.2 ± 12.6
(d)	(0, 3)	275	654.8 ± 35.7	669.5 ± 12.4	225	535.7 ± 35.7	524.2 ± 9.5
	(1, 1)	275	654.8 ± 35.7	681.2 ± 12.6	285	678.6 ± 35.7	681.2 ± 12.6

$$
\begin{aligned}
g(k_x, k_y) \rightarrow\ & T^{[\mathrm{TE,TM}]}(k_x, k_y)\, g(k_x, k_y) \\
=\ & \left| T^{[\mathrm{TE,TM}]}(k_x, k_y) \right| g(k_x, k_y) \\
& \times \exp\left\{ i \left[\phi_{\mathrm{Snell}}(k_x, k_y) + \phi_{\mathrm{GH}}^{[\mathrm{TE,TM}]}(k_x, k_y) \right] \right\}, \quad (3)
\end{aligned}
$$

where $T^{[\mathrm{TE,TM}]}$ are the transmission coefficients obtained by solving the electromagnetic Maxwell wave equations in the presence of stratified media. These coefficients contain the geometrical phase, ϕ_{Snell}, obtained by imposing the continuity of the electromagnetic field at dielectric/air interfaces (*1*) and the Goos-Hänchen phase, ϕ_{GH}, appearing in the Fresnel coefficients for incidence greater than the critical one (*2*). Observing that the effects on the beam propagation caused by the GH phase with respect to the ones caused by the Snell phase are proportional to $\lambda/\overline{AB}$, for the purpose of our investigation, without loss of generality, we can only consider the Snell

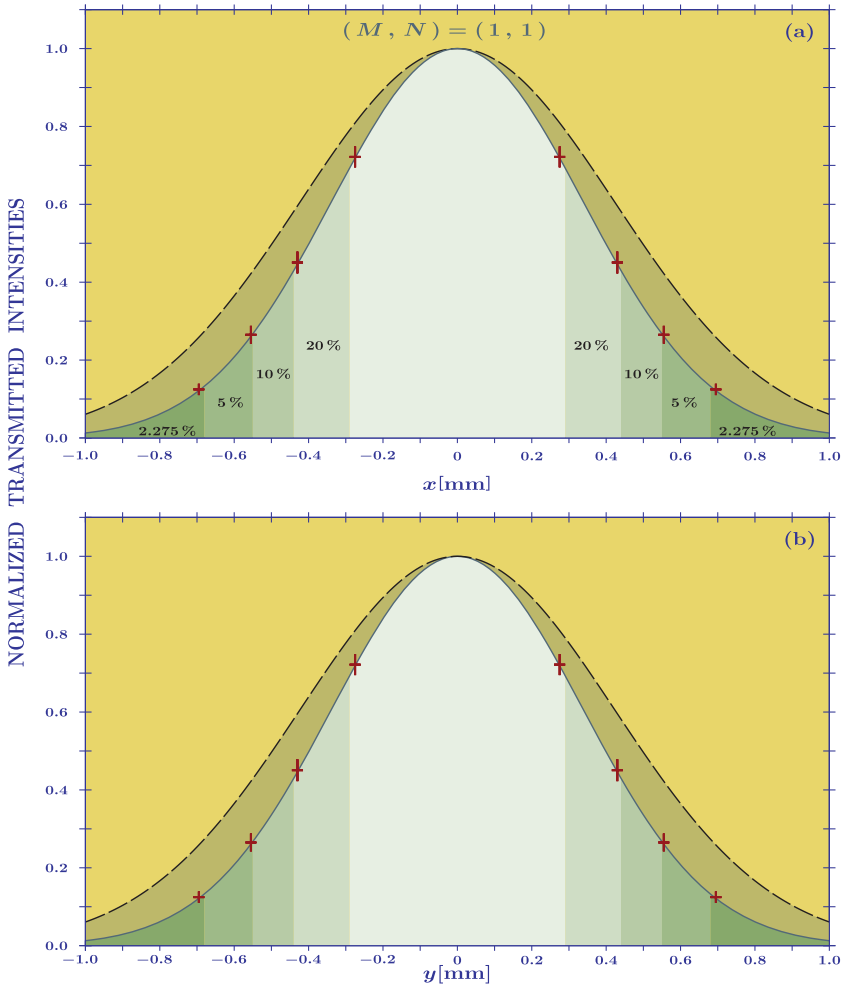

Figure 3. Transversal profiles of the normalized transmitted intensity. The dashed black lines represent the profiles for free propagation. The blue solid lines are the profiles for beams passing through the dielectric configuration $(M, N) = (1, 1)$. The symmetry between the transversal components x and y is recovered. It is also possible to see the axial spreading delay with respect to the free propagation. The experimental data show an excellent agreement with the theoretical curves.

Table 2. We give the experimental values of the transversal intensities, calculated by using Equation (20). The error in the x_{KM} and y_{KM} measurement is of 15μm.

KM	(M, N)	$x_{\mathrm{KM}}[\mu\mathrm{m}]$	$I_{\mathrm{Exp}}(x,0)[\%]$	$y_{\mathrm{KM}}[\mu\mathrm{m}]$	$I_{\mathrm{Exp}}(0,y)[\%]$
(a)	(0, 3)	685	12.3 ± 1.5	545	11.5 ± 1.6
	(1, 1)	695	12.5 ± 1.5	690	12.8 ± 1.5
(b)	(0, 3)	550	25.9 ± 2.3	440	24.4 ± 2.7
	(1, 1)	555	26.5 ± 2.3	550	27.1 ± 2.3
(c)	(0, 3)	425	44.7 ± 2.9	340	43.1 ± 3.5
	(1, 1)	430	45.1 ± 2.8	430	45.1 ± 2.8
(d)	(0, 3)	275	71.4 ± 2.8	225	69.2 ± 3.5
	(1, 1)	275	72.2 ± 2.7	285	70.5 ± 2.8

phase. The first-order terms are clearly responsible for the transversal lateral displacements. Indeed, they directly act on the transversal spatial phase $\exp[\, i\,(k_x\, x + k_y\, y\,)\,]$ modifying the centre of the incoming beam,

$$\{\, x_{\mathrm{inc}}, y_{\mathrm{inc}}\,\} = \{\, 0, 0\,\} \quad \rightarrow \quad \{\, x_{\mathrm{Snell}}, y_{\mathrm{Snell}}\,\} = \left\{ -\frac{\partial \phi_{\mathrm{Snell}}}{\partial k_x}, -\frac{\partial \phi_{Snell}}{\partial k_y} \right\}_{(0,0)}, \tag{4}$$

confirming the optical path predicted by the laws of geometrical optics(*1*). The Snell second-order terms act on the axial spatial phase $\exp[-i\,(k_x^2+k_y^2)\,z/2\,k\,]$ modifying the axial spreading in the transversal plane xz and yz (*11*),

$$\{\mathrm{w}(z)\,,\mathrm{w}(z)\}\quad\rightarrow\quad\left\{\mathrm{w}\left(z-k\,\frac{\partial^2\phi_{\mathrm{Snell}}}{\partial k_x^2}\right),\mathrm{w}\left(z-k\,\frac{\partial^2\phi_{\mathrm{Snell}}}{\partial k_y^2}\right)\right\}_{(0,0)}. \tag{5}$$

Consequently, propagation through dielectric blocks causes a symmetry breaking with respect to the free propagation and more important, as predicted in Ref. (*11*), a focalization like effect. The outgoing beam intensity, for incidence greater than the critical one, can then be expressed by

$$\mathrm{I}^{[\mathrm{TE,TM}]}(\boldsymbol{r},\theta)=\frac{I_0\,\mathrm{w}_0^2\,\left|T_\theta^{[\mathrm{TE,TM}]}\right|^{2\,(N+M)}}{\mathrm{w}(z-z_{\mathrm{Snell}}^{\perp})\,\mathrm{w}(z-z_{\mathrm{Snell}})}\times\exp\left\{-2\left[\frac{\left(x-x_{\mathrm{Snell}}\right)^2}{\mathrm{w}^2(z-z_{\mathrm{Snell}}^{\perp})}+\frac{\left(y-y_{\mathrm{Snell}}\right)^2}{\mathrm{w}^2(z-z_{\mathrm{Snell}})}\right]\right\}, \tag{6}$$

where

$$\left\{\left|T_\theta^{[TE]}\right|,\left|T_\theta^{[TM]}\right|\right\}=\left\{\frac{4\,n\,\cos\psi\,\cos\theta}{(\cos\theta\,+\,n\cos\psi)^2},\frac{4\,n\,\cos\psi\,\cos\theta}{(n\,\cos\theta\,+\,\cos\psi)^2}\right\} \tag{7}$$

are the Fresnel transmission coefficients for transverse electric (TE) and transverse magnetic (TM) waves(*5*). The angle ψ is obtained from the incidence angle θ by the Snell law, $\sin\theta=n\,\sin\psi$, and the angle φ (incidence at the down dielectric air interface) is given by $\psi+\frac{\pi}{4}$(*5*).

$$\left\{x_{\mathrm{Snell}},y_{\mathrm{Snell}}\right\}=\left\{M\,\frac{\cos\theta-\sin\theta}{\sqrt{2}},N\,\frac{\cos\theta-\sin\theta}{\sqrt{2}}\right\}\,\overline{BC} \tag{8}$$

is the centre of the beam obtained by the first-order term of the Taylor expansion of the Snell phase (confirming the optical path predicted by the ray optics) (*1*). $\overline{BC}=\sqrt{2}\,\tan\varphi\,\overline{AB}$ guarantees that the laser exit point from the dielectric block has the same height of the incoming one (*6*, *7*), and, finally,

$$\left\{z_{\mathrm{Snell}}^{\perp},z_{\mathrm{Snell}}\right\}=\left\{M\,f_\theta+N\,g_\theta,M\,g_\theta+N\,f_\theta\right\}\,\overline{AB}, \tag{9}$$

with

$$f_\theta=(\sin\theta\,+\,\cos\theta)\,\tan\varphi\,-\,\frac{\cos^2\theta}{n\,\cos^3\psi}\,(1\,+\,\tan\varphi),$$
$$g_\theta=\sin\theta\,+\,\cos\theta\,\tan\varphi\,-\,\frac{\cos^2\theta}{n\,\cos\psi}\,(1\,+\,\tan\varphi), \tag{10}$$

gives the axial spreading modifications due to the second-order contribution of the Snell phase expansion, for details, see ref. (*11*). For $N\neq M$,

$$z_{\mathrm{Snell}}^{\perp}\;\neq\;z_{\mathrm{Snell}}$$

which causes the transversal symmetry breaking.

Now that we are familiar with the mathematical formulation of the transmitted beam, it would be natural to consider a particular incidence angle to prepare the experiment. The choice of $\theta=\pi/4$ (see Figure 1) has the advantage of not modifying the centre of the beam (*8*),

$$\left\{x_{\mathrm{Snell}},y_{\mathrm{Snell}}\right\}=\{0,0\}\,. \tag{11}$$

For this incidence angle, we have

$$\{\sin\psi,\cos\psi,\sin\varphi,\cos\varphi\,\}=\left\{\frac{1}{\sqrt{2}\,n},\frac{\sqrt{2n^2-1}}{\sqrt{2}\,n},\frac{\sqrt{2n^2-1}+1}{2\,n},\frac{\sqrt{2n^2-1}-1}{2\,n}\right\}$$

and, consequently, the Fresnel coefficients (7) become

$$\left\{\left|T_{\pi/4}^{[TE]}\right|,\left|T_{\pi/4}^{[TM]}\right|\right\}=\left\{\frac{4\sqrt{2n^2-1}}{\left(1+\sqrt{2n^2-1}\right)^2},\frac{4n^2\sqrt{2n^2-1}}{\left(n^2+\sqrt{2n^2-1}\right)^2}\right\}. \tag{12}$$

It is possible to establish the axial modifications by knowing the number and the kind of blocks, (M,N), and the factors

$$f_{\pi/4}=\sqrt{2}\,\left(2n^2+\sqrt{2n^2-1}\right)/\left(2n^2-1\right)\quad\text{and}\quad g_{\pi/4}=\sqrt{2}. \tag{13}$$

The normalized intensity,

$$\mathcal{I}\,(\boldsymbol{r},\theta)=\frac{I^{[TE,TM]}(\boldsymbol{r},\theta)\mathrm{w}(z-z_{\mathrm{Snell}}^{\perp})\,\mathrm{w}(z-z_{\mathrm{Snell}})}{I_0\,\mathrm{w}_0^2\,\left|T_\theta^{[TE,TM]}\right|^{2\,(N+M)}},$$

is clearly independent of the polarization and for the incidence angle $\pi/4$ becomes

$$\mathcal{I}\left(\boldsymbol{r},\frac{\pi}{4}\right)=\exp\left\{-2\left[\frac{x^2}{\mathrm{w}^2[z-(M f_{\pi/4}+N g_{\pi/4})\,\overline{AB}\,]}+\frac{y^2}{\mathrm{w}^2[z-(M g_{\pi/4}+N f_{\pi/4})\,\overline{AB}\,]}\right]\right\}. \tag{14}$$

The choice of a configuration with a number of blocks $M = N$ allows to recover the transversal symmetry. In this case, the outgoing beam will be a symmetric gaussian beam and its width will be reduced with respect to the width of a beam propagating in the free space (focalization like effect caused by the propagation through the dielectric blocks).

3. Experimental evidence of transversal symmetry breaking

Before discussing the experimental data, let us describe the experimental setup used to observe the transversal symmetry breaking and the axial spreading modification. The incoming beam was a TM polarized gaussian DPSS laser (the choice of a particular polarization does not influence the profile modifications) with a power of 1, 5 mW, with a wavelength

$$\lambda = 532\,\mathrm{nm},$$

and focused, by a lens of focal length $f = 50$ cm, in order to obtain a beam waist radius

$$\mathrm{w}_0 = (\,79.0 \pm 1.5\,)\,\mu\mathrm{m}.$$

The beam parameters were determined by applying the knife-edge method along the beam path (*18*). Recalling that

$$\mathrm{w}(z)=\mathrm{w}_0\sqrt{1+\left(\frac{\lambda z}{\pi \mathrm{w}_0^2}\right)^2}$$

and observing that

$$\begin{aligned}\frac{\sigma[\mathrm{w}(z)]}{\mathrm{w}(z)}&=\sqrt{\left[\frac{\partial \mathrm{w}(z)}{\partial \mathrm{w}_0}\,\sigma(\mathrm{w}_0)\right]^2+\left[\frac{\partial \mathrm{w}(z)}{\partial z}\,\sigma(z)\right]^2}\Big/\,\mathrm{w}(z)\\&=\sqrt{\left[2\frac{\mathrm{w}_0}{\mathrm{w}(z)}-\frac{\mathrm{w}(z)}{\mathrm{w}_0}\right]^2\sigma^2(\mathrm{w}_0)+\left[1-\frac{\mathrm{w}_0^2}{\mathrm{w}^2(z)}\right]\left(\frac{\lambda}{\pi\,\mathrm{w}_0}\right)^2\sigma^2(z)}\Big/\,\mathrm{w}(z)\\&\approx\left[1-2\frac{\mathrm{w}_0^2}{\mathrm{w}^2(z)}\right]\frac{\sigma(\mathrm{w}_0)}{\mathrm{w}_0}[\,\mathrm{w}(z)>\sqrt{2}\,\mathrm{w}_0\,],\end{aligned} \tag{15}$$

for free propagation, at the power meter located at

$$z_{\mathrm{PM}} = (\,39.5 \pm 0.1\,)\,\mathrm{cm},$$

we should find the following beam width

$$\mathrm{w}_{\mathrm{Teo}}^{\mathrm{Free}} = (\,850.4 \pm 15.9\,)\,\mu\mathrm{m}. \tag{16}$$

Each dielectric block used in the experiment had a refractive index $n = 1.515$ (BK7) and dimensions

$$\underbrace{(\,91.5 \pm 0.5\,)\,\mathrm{mm}}_{\overline{BC}} \times \underbrace{(\,20.0 \pm 0.5\,)\,\mathrm{mm}}_{\overline{AB}} \times (\,14.0 \pm 0.5\,)\,\mathrm{mm}$$

see Figure 1(a) and (b). The incoming beam propagates along the z-axis (see Figure 1) and forms with the left interface an angle of $\theta = \pi/4$ in both the (a) and (b) configurations. To guarantee that the transmitted beam coming out of the dielectric block at the same height of the incident point,

$$\overline{BC}=\sqrt{2}\,\frac{\sqrt{2\,n^2-1}+1}{\sqrt{2\,n^2-1}-1}\;\overline{AB}.$$

The blocks faces are anti-reflection coated to reduce unwanted internal reflections.

In order to investigate the axial spreading modification and the transversal symmetry breaking, we used two different block configurations. Figure 1(a) shows a block in which the plane of propagation is the y-z plane. This dielectric structure corresponds to the configuration $(M, N) = (0, 1)$. By rotating the block clockwise along the z-axis with an angle $\pi/2$, we get a dielectric structure in which the plane of propagation is the $x-z$ plane, as shown in Figure 1(b). This dielectric structure corresponds to the configuration $(M, N) = (1, 0)$. In Figure 1(c), we have the configuration $(M, N) = (2, 1)$, i.e. two blocks with a plane of propagation in the x–z plane and one with a plane of propagation in the y-z plane. The order is not relevant and the transversal profiles will be the same for all possible permutations of the blocks. The symmetry

is recovered after the beam passes through the first two blocks with a different plane of propagation. After passing through the last block, the transversal symmetry breaking acts principally on the x-axis reverting what happened after the first block. By using

$$\left(\mathrm{w}_{\mathrm{Teo}}^{\mathrm{Snell},\perp}, \mathrm{w}_{\mathrm{Teo}}^{\mathrm{Snell}}\right) = \Big(\mathrm{w}[z_{\mathrm{PM}} - (M f_{\pi/4} + N g_{\pi/4})\,\overline{AB}\,], \times \mathrm{w}[z_{\mathrm{PM}} - (M g_{\pi/4} + N f_{\pi/4})\,\overline{AB}\,]\Big), \tag{17}$$

we can give the theoretical predictions of the outgoing beam widths at the power meter

$$\left(\mathrm{w}_{\mathrm{Teo}}^{\mathrm{Snell},\perp}, \mathrm{w}_{\mathrm{Teo}}^{\mathrm{Snell}}\right) = \begin{cases} (669.5 \pm 12.4, 524.2 \pm 9.5)\ \mu\mathrm{m} & (M,N) = (0,3) \\ (681.2 \pm 12.6, 681.2 \pm 12.6) & (1,1) \end{cases}, \tag{18}$$

where the errors were obtained using Equation (15).

The experimental widths were calculated by

$$\left(\mathrm{w}_{\mathrm{Exp}}^{\mathrm{Snell},\perp}, \mathrm{w}_{\mathrm{Exp}}^{\mathrm{Snell}}\right) = \left(x_{\mathrm{KM}}, y_{\mathrm{KM}}\right)/\alpha, \tag{19}$$

where x_{KM} and y_{KM} were found by the knife-method for

$$2.275\%-97.725\%\ \ (\mathrm{a}),\quad 5\%-95\%\ \ (\mathrm{b}),\quad 10\%-90\%\ \ (\mathrm{c}),\quad 20\%-80\%\ \ (\mathrm{d}),$$

and the α factor obtained by

$$\sqrt{\frac{2}{\pi}}\int_{-\alpha}^{+\alpha} \mathrm{d}r\, e^{-2r^2} = 95.45\%\ \ (\mathrm{a}),\quad 90\%\ \ (\mathrm{a}),\quad 80\%\ \ (\mathrm{a}),\quad 60\%\ \ (\mathrm{a}),$$

which implies

$$\alpha = 1\ \ (\mathrm{a}),\quad 0.82\ \ (\mathrm{b}),\quad 0.64\ \ (\mathrm{c}),\quad 0.42\ \ (\mathrm{d}).$$

The experimental data for x_{KM} and y_{KM} and the corresponding beam widths $\mathrm{w}_{\mathrm{Exp}}^{\mathrm{Snell},\perp}$ and $\mathrm{w}_{\mathrm{Exp}}^{\mathrm{Snell}}$ are listed in Table 1. The experimental widths are in agreement with the theoretical predictions given in Equation (18).

Using the measurements done by the knife-method, we can also obtain the intensity at the power meter,

$$I_{\mathrm{Exp}}(x,y) = \exp\left\{-2\left[\left(\frac{x_{\mathrm{KM}}}{\mathrm{w}_{\mathrm{Teo}}^{\mathrm{Snell},\perp}}\right)^2 + \left(\frac{y_{\mathrm{KM}}}{\mathrm{w}_{\mathrm{Teo}}^{\mathrm{Snell}}}\right)^2\right]\right\}, \tag{20}$$

and its errors,

$$\frac{\sigma[I_{\mathrm{CAM}}^{\mathrm{Exp}}(x,0)]}{I_{\mathrm{CAM}}^{\mathrm{Exp}}(x,0)} = 4\,\frac{x}{\mathrm{w}_{\mathrm{CAM}}^{\mathrm{Snell},\perp}}\sqrt{\left[\frac{\sigma(x)}{\mathrm{w}_{\mathrm{CAM}}^{\mathrm{Snell},\perp}}\right]^2 + \left[\frac{x\,\sigma(\mathrm{w}_{\mathrm{CAM}}^{\mathrm{Snell},\perp})}{\mathrm{w}_{\mathrm{CAM}}^{\mathrm{Snell},\perp\ 2}}\right]^2},$$
$$\frac{\sigma[I_{\mathrm{CAM}}^{\mathrm{Exp}}(0,y)]}{I_{\mathrm{CAM}}^{\mathrm{Exp}}(0,y)} = 4\,\frac{y}{\mathrm{w}_{\mathrm{CAM}}^{\mathrm{Snell}}}\sqrt{\left[\frac{\sigma(y)}{\mathrm{w}_{\mathrm{CAM}}^{\mathrm{Snell}}}\right]^2 + \left[\frac{y\,\sigma(\mathrm{w}_{\mathrm{CAM}}^{\mathrm{Snell}})}{\mathrm{w}_{\mathrm{CAM}}^{\mathrm{Snell}\ 2}}\right]^2}. \tag{21}$$

These intensity values are listed in Table 2 and were used in the plots of Figure 2, configuration $(M,N) = (0,3)$, and Figure 3, configuration $(1,1)$, to compare the experimental data with the theoretical curves (blue solid lines) obtained by Equation (14). The agreement is excellent and confirms the theoretical predictions. The dashed black lines represent the beam intensity for free propagation. As can be seen in all three configurations, we have a clear spreading delay of the laser passing through dielectric blocks. In Figure 2, we can see a maximal breaking of symmetry between the transversal coordinates. The symmetry is recovered in Figure 3 where $M = N = 1$.

4. Conclusions

The Goos-Hänchen phase has been the matter of studies since the fifties (*2*, *3*). The Snell phase, often forgotten, has recently been used as an alternative way to obtain the optical path predicted by geometrical optics (*1*) and, even more important, to predict the axial spreading modification and the breaking of symmetry in the transversal profiles of laser propagating through dielectric blocks (*11*).

In this paper, we have experimentally tested the theoretical predictions, for an incidence angle of $\pi/4$, and found an excellent agreement with the analytical formula given by literature (*11*). This excellent agreement of experimental data and theory can be regarded as a convincing proof of the importance to use the Snell phase in order to correctly describe the propagation of optical beams through dielectric blocks, on one hand, and of the possibility to use dielectric structures to control the laser beam profile, on the other hand. Indeed, this profile modification technique, allowing to focus the beam and to act on its transversal symmetry, is better than using a simple lens.

Future studies could test the formula at different angles and observe, in particular, the results in the proximity of the critical angle where analytical formulas cannot be obtained and where the Goos-Hänchen phase could play a relevant role. In this case, the experimental data should be compared with numerical calculations. We also expect phenomena of transversal symmetry breaking in Herimite and Laguerre-Gauss beams propagating through dielectric blocks.

Acknowledgements

The authors thank the CNPq, FAPERJ and PROPPI-UFF for the financial support. They also thank Prof. Luis Araújo e Dr. Manoel P. Araújo for useful comments and stimulating conversations and Dr. Rita K. Kraus for a critical reading of the manuscript. The authors are greatly indebted with an anonymous referee who, with his suggestions and observations, helped to improve the final version of the paper.

Disclosure statement

No potential conflict of interest was reported by the authors.

References

(1) Carvalho, S.A.; De Leo, S. The use of the stationary phase method as a mathematical tool to determine the path of optical beams. *Am. J. Phys.* **2015,** *83,* 249–255.
(2) Goos, F.; Hänchen, H. Ein neuer und fundamenta ler Versuch zur totalreflexion [A new and fundamental experiment for total reflection]. *Ann. der Physik* **1947,** *436,* 333–346.
(3) Artmann, K. Berechnung der Seitenversetzung des Totalreflektierten Strahles [Calculation of the lateral shift of totally reflected beam]. *Annalen der Physik (Leipizig)* **1948,** *437,* 87–102.
(4) Bliokh, K.Y.; Aiello, A. Goos-Hänchen and Imbert-Fedorov beam shifts: an overview. *J. Opt.* **2013,** *15,* 014001–16.
(5) Araújo, M.P.; Carvalho, S.A.; De Leo, S. The frequency crossover for the Goos-Hänchen shift. *J. Mod. Opt.* **2013,** *60,* 1772–1780.
(6) Araújo, M.P.; Carvalho, S.A.; De Leo, S. The asymmetric Goos-Hänchen effect. *J. Opt.* **2014,** *16,* 015702–7.
(7) Araújo, M.P.; Carvalho, S.A.; De Leo, S. Maximal breaking of symmetry at critical angles and a closed-form expression for angular deviations of the Snell law. *Phys. Rev. A* **2014,** *90,* 033844–11.
(8) Arajo, M.; De Leo, S.; Maia, G. Closed form expression for the Goos-Haenchen lateral displacement. *Phys. Rev. A* **2016,** *93,* 023801-9.
(9) Born, M.; Wolf, E. *Principles of Optics*, Cambridge University Press: Cambridge, 1999.
(10) Saleh, B.E.A.; Teich, M.C. *Fundamentals of Photonics*, Wiley: NJ, 2007.
(11) Araujo, M.P.; De Leo, S.; Lima, M. Transversal symmetry breaking and axial spreading modification for gaussian optical beams. *J. Mod. Opt.* **2016,** *63,* 417–427.
(12) Lugiato, L.A.; Grangier, Ph. Improving quantum-noise reduction with spatially multimode squeezed light. *J. Opt. Soc. Am. B* **1997,** *14,* 225–231.
(13) Sauvan, C.; Lalanne, P.; Hugonin, J.P. Slow-wave effect and mode-profile matching in photonic crystal microcavities. *Phys. Rev. B* **2005,** *71,* 165118.
(14) Cowan, A.R.; Young, J.F. Mode matching for second-harmonic generation in photonic crystal waveguides. *Phys. Rev. B* **2002,** *65,* 085106.
(15) Grimm, R.; Weidemüller, M.; Ovchinnikov, Y.B. Optical dipole traps for neutral atoms. *Adv. At. Mol. Opt. Phy.* **2000,** *42,* 95–170.
(16) Meyrath, T.P.; Schreck, F.; Hanssen, J.L.; Chuu, C.S.; Raizen, M.G. Bose Einstein condensate in a box. *Phys. Rev. A* **2005,** *71,* 041604(R).
(17) Meyrath, T.P.; Schreck, F.; Hanssen, J.L.; Chuu, C.S.; Raizen, M.G. A high frequency optical trap for atoms using Hermite-Gaussian beams. *Opt. Express* **2005,** *13,* 2843–2851.
(18) Magnes, J.; Odera, D.; Hartke, J.; Fountain, F.; Florence, L.; Davis, V. *Quantitative and Qualitative Study of Gaussian Beam Visualization Techniques*, 2006. http://arxiv.org/abs/physics/0605102.